Experimental Methods for Testing the Tensile Properties of Single Vaginal Smooth Muscle Cells

Zachary D. Miller

Dissertation submitted to the Faculty of the

Virginia Polytechnic Institute and State University

in partial fulfillment of the requirements for the degree of

Master of Science

in

Engineering Mechanics

Raffaella De Vita, Chair

Sunghwan Jung

Vincent M. Wang

May 9, 2018

Blacksburg, Virginia

Keywords: Biomechanics, Vagina, Smooth Muscle, Cell Mechanics, Pelvic Organ Prolapse

Copyright 2018, Zachary D. Miller

Experimental Methods for Testing the Tensile Properties of Single Vaginal Smooth Muscle Cells

Zachary D. Miller

(ABSTRACT)

Improving treatment and prevention of pelvic organ prolapse, a disorder affecting up to half of parous women, requires thorough mechanical analysis of the vagina and other endopelvic structures at the cellular level. In this study, we tested single vaginal smooth muscle cells (SMCs) to quantify their elastic moduli. Cells were enzymatically isolated from vaginal walls of freshly sacrificed, virgin Long Evans rats and cultured using well-established methods. A custom-built experimental setup was used to perform tensile tests. Micropipettes were fabricated to serve as cantilever-type load cells, which were coated in cellular adhesive. Two pipettes applied tension to SMCs until adhesion between the cell and a pipette failed. During mechanical testing, images of SMCs were collected and translated into strain and stress. Specifically, force/stress data were calculated using Euler-Bernoulli Beam Theory and by making simplifying geometric assumptions. The average initial and total elastic moduli (mean $\pm$ SEM) for single vaginal SMCs were 6.06 $\pm$ 0.26 kPa and 5.4 $\pm$ 0.24 kPa, respectively, which is within the range reported for other types of SMCs, mainly airway and vascular, of various species. This protocol can and will be applied to further investigate mechanics of single cells from the pelvic region with independent variables such as parity, age, body mass index, and various stages of POP. Results of these experiments will provide critical information for improving current treatments like drug therapies, surgical procedures, medical grafts and implants, and preventative practices like stretching and exercise techniques.

Experimental Methods for Testing the Tensile Properties of Single Vaginal Smooth Muscle Cells

Zachary D. Miller

(GENERAL AUDIENCE ABSTRACT)

Pelvic organ prolapse, the descent of the pelvic organs into the vagina or rectum, affects up to half of women who have undergone childbirth. Improving treatment requires thorough analysis and quantification of the vagina and other endopelvic structures at the tissue and cellular levels. In this study, we tested single vaginal smooth muscle cells (SMCs) to quantify their elastic moduli. A custom-built experimental setup was used to pull single SMCs using two micropipettes. By measuring the deflection of a flexible pipette, we calculated force applied to each cell and the corresponding strain. The pipettes were coated in cellular adhesive and applied tension to SMCs until adhesion between the cell and a pipette failed. During mechanical testing, images of SMCs were collected and translated into strain and stress. Specifically, force/stress data were calculated using Euler-Bernoulli Beam Theory and by making simplifying geometric assumptions. The average initial and total elastic moduli (mean $\pm$ SEM) for single vaginal SMCs were 6.06 ± 0.26 kPa and 5.4 ± 0.24 kPa, respectively, which is within the range reported for other types of SMCs, mainly airway and vascular, of various species. This protocol can and will be applied to further investigate mechanics of single cells from the pelvic region with independent variables such as pregnancy, age, body mass index, and various stages of POP. Results of these experiments will provide critical information for improving current treatments like drug therapies, surgical procedures, medical grafts and implants, and preventative practices like stretching and exercise techniques.

This work is dedicated to friends and family that have supported and encouraged me during my academic pursuits.

Thank you to my parents, Chris and BJ Miller, for supporting me during my education. You have set excellent examples of how to be good and successful and I love and respect you both so much.

Thank you to my sister, Logan, for being a great role model and always sharing your insightful perspective in all situations. I am glad we grew up together and that we remain good friends.

Thank you to Tessa, for helping me strive to be a better person and live a happier, healthier life. Without you, this work would have been completed much sooner.

Lastly, thanks to Spike for always being happy to see me and for your endless energy.

Acknowledgments

This work was supported by NSF award #1511603. Thank you to my advisor Dr. Raffaella De Vita for being incredibly knowledgeable and encouraging during my participation in the STRETCH lab. It has been a pleasure working with such a great advisor and the other great students she recruits. Thank you also to my committee members, Dr. Vincent Wang and Dr. Sunny Jung, for their guidance and help producing this thesis. I would also like to acknowledge Dr. Adwoa Baah-Dwomoh and Ph.D. candidate Jeffrey McGuire for their training and advice as supportive members of the STRETCH laboratory.

Contents

List of Figures

List of Tables

Chapter 1

Introduction

Pelvic organ prolapse (POP), the descent of pelvic organs into the vagina or rectum, is a common disorder affecting up to half of parous women in the United States. Surgery is offered as treatment for the disorder with over $1 billion of direct annual medical costs in the US [33]. The success rate for surgery is quite low: reoperation is required in nearly one out of three patients [58]. The etiology of POP is multifactorial and not fully understood, but certainly involves changes in the material characteristics of endopelvic tissues and pelvic organs, like the vagina. Among others, two risk factors for POP include pregnancy and menopause, during which the pelvic organs and tissue undergo physiological and mechanical changes [60]. However, the extent to which these changes are a cause or consequence of POP remains to be determined.

Studies have shown that protein regulating genes [6], extracellular collagen [45, 48], and smooth muscle content and proteins [4, 5] are significantly different between vaginal biopsies of healthy patients versus those with POP. Additionally, women with POP have a lower ratio of smooth muscle in the vaginal wall and surrounding endopelvic structures than women without POP [33], at least partially due to accelerated smooth muscle cell (SMC) apoptosis

[59]. These alterations in SMCs occur with age or physical trauma like childbirth, high body mass index (BMI), or inadequate surgical grafts used for surgical POP treatment (Figure 1.1). Hormonal changes also occur in conjunction with pregnancy and menopause, but the effect of these hormones on pelvic cells is not completely understood. Hormone therapy and repetitive mechanical loading has been shown to lower cell proliferation [63] and significantly influence DNA content and genetic expression [50, 65, 67].

Pelvic fibroblasts and SMCs from women with POP or treated with hormones that are abundant during pregnancy and menopause exhibit less contraction [35], produce more collagen [71], and produce stiffer extracellular matrices [51] when compared to cells from healthy patients. Tissues more densely populated with stiff components like collagen have significantly different mechanical behavior. Some studies have investigated this mechanical alteration at the tissue level, but no studies have characterized material properties of single vaginal cells.

Although vaginal SMCs have not been mechanically studied, research has been conducted to investigate mechanical characteristics of other SMCs using various experimental methods [29]. Successful techniques include the use of aspirating pipettes [30, 36], carbon fiber pipettes [22, 23, 24, 28, 57, 70], micropillar arrays [40, 43], elastic substrates [66], and microbeads which respond to light or magnetic fields [25, 27]. The main objective of these experiments was to describe the material response of single SMCs, including the influence of substrate type, phenotype, soluble signaling factors, and activation. In these tests, cells have been carefully cultured and prepared for testing. Often, individual cells are chemically removed from the substrate to which they are attached using a protease like trypsin. This can, however, compromise their cytoskeletal structure which is ultimately responsible for the mechanical behavior of cells. The actin and myosin filaments comprising the cytoskeleton are typically aligned with the major axis of the cell but, once the cells are treated with trypsin, these filaments change configuration and assume random orientations leading to a

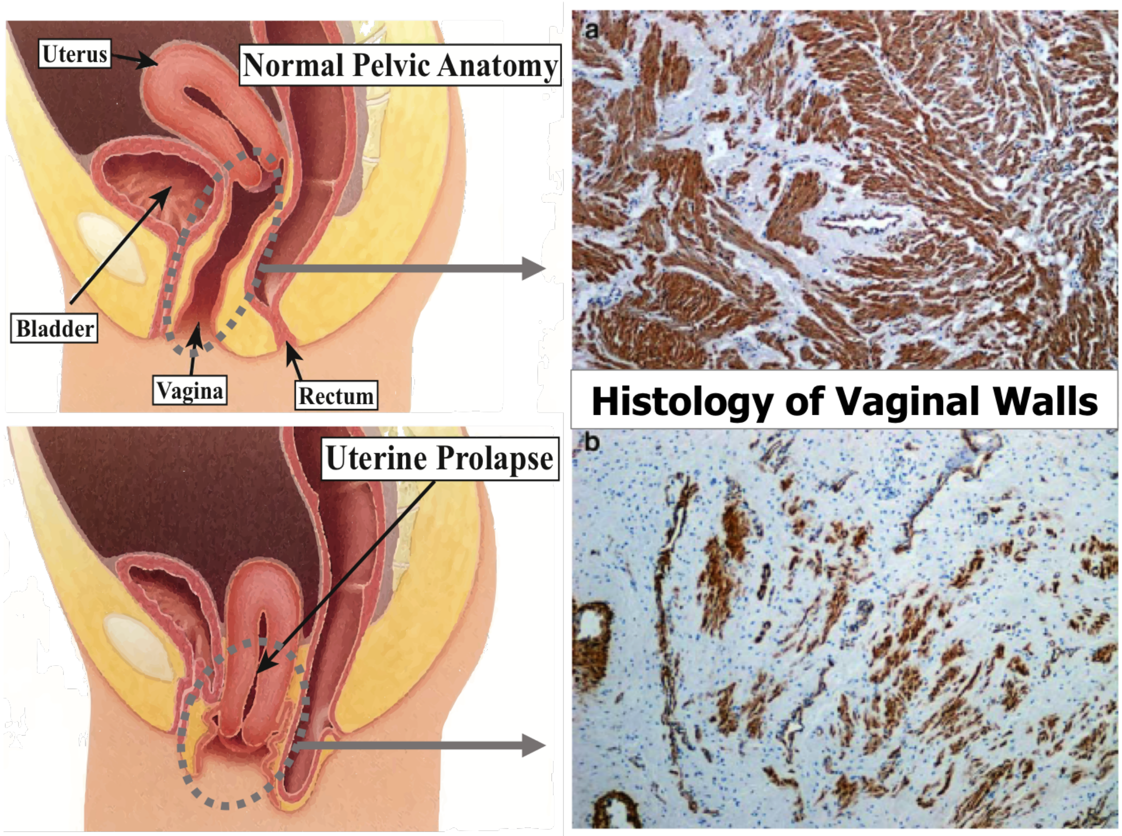

Figure 1.1: Graphical representation of uterine prolapse with corresponding histological changes in the vaginal wall of humans. Uterine prolapse is one type of pelvic organ prolapse. Tissue biopsies from a healthy patient (top) and a patient with prolapse (bottom) were stained for smooth muscle α-actin [59]. Vaginal smooth muscle content reduces from roughly 45% in healthy patients to approximately 15% in patients suffering from uterine prolapse.

new spherically shaped cell configuration [42, 44]. Ideally, cells should be pulled directly from the substrate, without using trypsin, and immediately tested to preserve the most similar *in situ* conditions. It should be noted, however, that during basic mechanical experiments, no significant difference in elasticity was observed between trypsin treated, round, suspended vascular SMCs and elongated SMCs that are pulled from the substrate [41]. Similarly, the media in which cells are tested may affect their mechanical properties. Calcium (Ca^{2+}) and magnesium (Mg^{2+}) are two common media ingredients that have been shown to influence the mechanical response of myocytes [55, 68]. Although Hank's Balanced Salt Solution ($HBSS^{-}$)

is a common media used for testing single cells, there are no publications that report its effect on the tensile properties of SMCs. Finally, the subculture passage number of the cells can also influence the results of mechanical tests that are conducted on single cells. Each subculture of a cell population increases its passage number by one, beginning with zero for freshly isolated cells from tissue. Passage number is loosely correlated to cellular phenotype in SMCs. The phenotype can differentiate along a continuum with extremes named "contractile" and "synthetic," both of which exist *in vivo* and have unique genetic and proteomic expressions [2, 52]. Many factors have been identified which influence the differentiation process, including population density [8], mechanical stimulation [7, 65, 69], soluble signaling factors [16, 47], extracellular matrix (ECM) or substrate [18], and surrounding endothelial cells [49]. Studies have shown that vascular SMCs of different phenotypes exhibit significantly different elastic moduli [30, 37, 41, 44].

Of the above cited methods for testing single cells, the most successful involves the use of glass micropipettes to hold and stretch cells [29, 31, 39, 42]. The glass micropipettes are used also as cantilever-type load cells. The micropipettes are relatively inexpensive to fabricate compared to micropillars or elastic substrates. Moreover, the dimensions of the micropipettes can be carefully tailored to the specific experiments and different adhesives such as urethane resin [44], APTES and Poly-D-Lysine [62], Polycel [53], and Cell-Tak [37], which can be used to clamp the cells.

The purpose of this thesis is to establish a new protocol for testing the elastic modulus of single vaginal SMCs. This protocol can and will be extended to investigate material differences in vaginal cells that are likely caused by parity, age, BMI, and various stages of POP. The proposed methods include the use of custom-made glass micropipettes as force sensors to quantify material properties of single vaginal SMCs. In order to design the experimental protocol, we considered the effect of the cell exposure time to testing medium and the cell passage number on the mechanical properties of vaginal SMCs. The goal was to determine whether or not these experimental conditions should be controlled in future experiments. Specifically, we investigated the effect of exposure time to HBSS^{-} and the effect of passage number. Although the current protocol was designed for testing the mechanical properties of vaginal SMCs, it can be applied to other cells of the pelvic organs and tissues. Experiments on the mechanics of the SMCs will provide critical information for improving current treatments like drug therapies, surgical procedures, medical grafts, implants, and preventative practices like healthy stretching and exercise techniques for POP. The results of current and future studies on single vaginal SMCs will advance our limited knowledge of POP and guide the development of new cellular-based bio-technologies for POP prevention and treatment.

Chapter 2

Methods & Materials

A healthy vaginal wall in humans is approximately 50% smooth muscle and the remaining tissue is dominated by collagen and the fibroblasts which help produce it [5, 59]. The current study uses rats as an animal model because they are accessible, easily managed, and are histologically similar to humans in regards to their pelvic tissues and organs [1, 38].

2.1 Isolation & Culture

Smooth muscle cells were enzymatically isolated from full-length biopsies of the vaginal wall of nulliparous Long Evans rats (10-13 weeks of age) using Liberase TM (Sigma-Aldrich), which is a mix of collagenase isoforms I and II and neutral protease enzymes. After reconstituting Liberase TM with injection-quality sterile water to the recommended concentration (2.5 mg mL^{-1}), single-use aliquots (100 μL) were used for cell digestion. For digestion, each aliquot was mixed with 1900 μL sterile PBS in a 15 mL centrifuge tube and cells were isolated using well-established methods [10, 34].

Tissue biopsies were obtained from freshly sacrificed rats, placed in a container with phosphate buffered saline (PBS) and immediately moved to a biological safety cabinet to maintain a sterile environment. They were then washed in a conical tube with sterile PBS, deposited into a cell tray with fresh PBS, and mechanically minced into the smallest manageable pieces to maximize surface exposure to Liberase TM. Tissue pieces were then transferred to the centrifuge tube with Liberase TM, sealed with parafilm, and placed in a 37°C hot bath for three hours with gentle agitation. After the hot bath, fresh full media was added for 10 mL of total liquid. The conical tubes were centrifuged at 28°C and 120× gravity for 10 minutes to create a cell pellet. Using a Pasteur pipette, excess liquid was removed without disturbing the cell pellet at the bottom of the tube. The cells were then dispersed into full media by triturating, or pipetting up and down, for 20-30 repetitions to create a relatively uniform mixture. The contents were transferred to 25 mL flasks for further passaging and placed in an incubator at 37°C with 5% CO_2. The full media was composed of Dulbecco's Modified Eagle's Medium (DMEM) (High Glucose - Pyruvate, ThermoFisher), 10% fetal bovine serum (FBS) (US Origin, ThermoFisher), and 1% penicillin-streptomycin (Pen-Strep) (5000 U mL^{-1}, ThermoFisher).

After a day or two, growth of the primary vaginal SMCs was confirmed and the cells were either passaged into 7 mL petri dishes for testing (passage 1) or seeded into another 25 mL flask for further passaging (passages 4-6). To passage, the cells were washed twice with PBS, submerged in trypsin-EDTA (0.25%, ThermoFisher), and then placed in the incubator for 3-5 minutes. After visually confirming the cells were detached and suspended, full media was added to neutralize the trypsin and the cells were dispersed into a petri dish for testing or a flask to continue passaging. Immediately before testing, full media was substituted with $HBSS^{-}$.

2.2 Equipment

In order to test single SMCs isolated from rat vaginal walls, we used a custom-built testing setup primarily composed of an inverted microscope (Olympus IX51), two 3-axis micromanipulators (PCS-5000 Series, Burleigh) with patch clamp micromanipulation power supply (PCS-PS60, Burleigh), a piezoelectric actuator (P-6014SL, PI), a thermoplate (TP-S, Tokai Hit), a high-resolution camera (DCC1645c-HQ, ThorLabs), and an HP EliteBook laptop (Figure 2.1). Our setup is capable of recording image data with a spatial resolution of 90 nm and a temporal resolution as high as 15 frames per second.

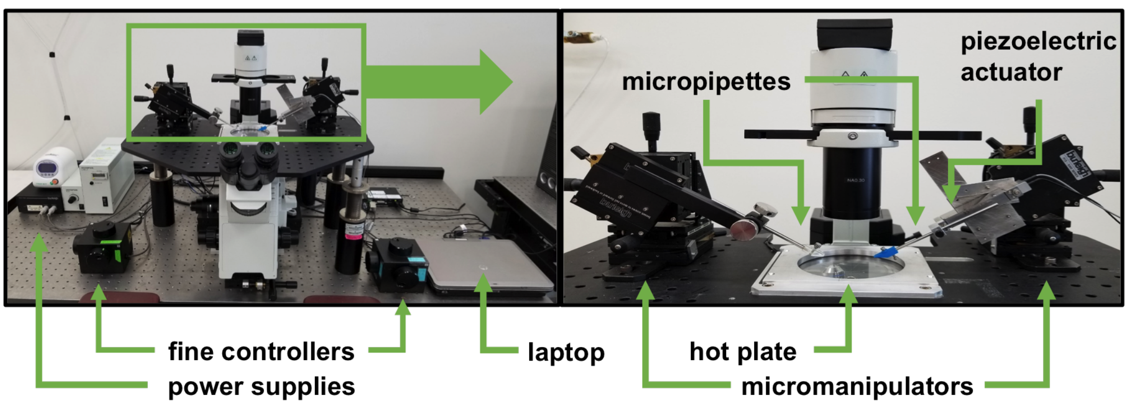

Figure 2.1: Complete experimental setup (left) with close-up view of stage (right).

2.2.1 Micropipettes & Force Calibration

Micropipettes were fabricated from solid glass rods originally 1 mm in diameter (GR100-4, World Precision Instruments) with an elastic modulus of 64 GPa. The rods were first pulled using a micropipette puller (Flaming/Brown P-1000, Sutter Instruments) to taper the rod at one end. Then, a microforge (Stoelting) was used to bend the pipettes 25° relative to the original axial direction, so the non-tapered end could be attached to the micromanipulators while the free end remained parallel to the substrate.

Two types of micropipettes were created for the experiments. Stiff pipettes had tip diameters of roughly 35 μm and 750 μm of cantilever length, while flexible pipettes had tip diameters (D_1)of only 9 μm and cantilever lengths (L) of 3,500 μm. Because the stiff pipettes were orders of magnitude stiffer than the flexible pipettes, it was assumed that, during testing, they had no displacement relative to the controlled displacement of the piezoelectric actuator.

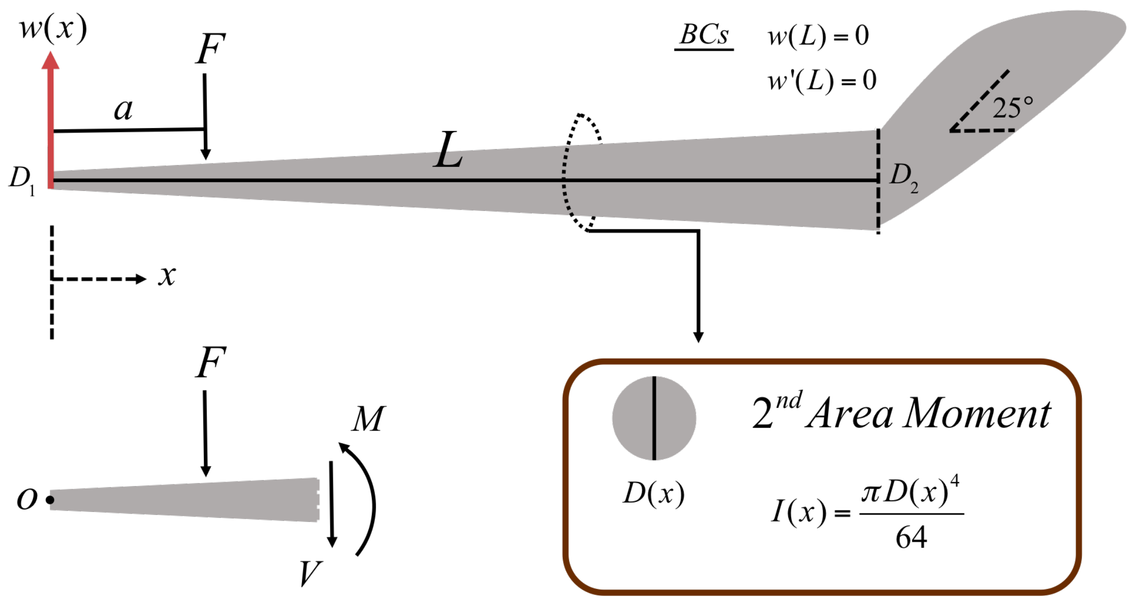

Figure 2.2: Standard beam problem (top) and FBD (bottom left), solved using Euler-Bernoulli Beam Theory with fixed-displacement and no-slope boundary conditions at the 25° bend in the pipette. It was assumed that the taper for all pipettes is linear and that the cross-section is circular along the entire cantilever.

In order to measure force applied to the cell with the flexible pipettes, we solved the Euler-Bernoulli beam equation for a tapered cantilever by analyzing the free body diagram (Figure 2.2). Using the convention that counter-clockwise moments (M) are positive, we obtained

$$\sum F = 0 = -F - V \tag{2.1}$$

$$V = -F \tag{2.2}$$

$$\sum M_o = 0 = -Fa - Vx + M = -Fa + Fx + M \tag{2.3}$$

$$M = -F(x - a) \tag{2.4}$$

The Euler-Bernoulli Beam Theory states

$$EI(x)\frac{d^2w(x)}{dx^2} = M = -F(x - a) \tag{2.5}$$

where E is the elastic modulus of the pipette, $I(x)$ is the 2^{nd} area moment of inertia, $w(x)$ is the displacement of the pipette, F is the applied point load, and a is the distance from the cantilever tip to the point load. It should be noted that the equation is solved for pipette displacement as a function of x, while also using the 2^{nd} area moment as a function of x, because of the changing cross-sectional area along the cantilever. Specifically,

$$I(x) = \frac{\pi D(x)^4}{64} = \frac{\pi}{64}\left(D_1 + \frac{x}{L}(D_2 - D_1)\right)^4 \tag{2.6}$$

where $D(x)$ is the cross-sectional diameter of the pipette as a function of x, D_1 is the diameter of the pipette tip, D_2 is the diameter of the pipette at the 25° bend, and L is the length of the cantilever, as labelled in the free body diagram (Figure 2.2). We substituted Equation 2.6 into Equation 2.5 and assumed boundary conditions at the pipette bend to obtain the governing equations of our pipette cantilever

$$E\frac{\pi}{64}\left(D_1 + \frac{x}{L}(D_2 - D_1)\right)^4 \frac{d^2w}{dx^2} = M = -F(x-a) \tag{2.7}$$

with boundary conditions

$$w(L) = 0 \tag{2.8}$$

$$w'(L) = 0 \tag{2.9}$$

Using Mathematica to solve Equation 2.7 with boundary conditions defined by Equation 2.8 and Equation 2.9, we obtained

$$w(x) = \frac{32F}{3\pi E}\left(\frac{L(L-x)^2(a(2D_1(L-x)+D_2(L+2x))+L(2D_1(x-L)-3D_2x))}{D_2^3(D_1(L-x)+D_2x)^2}\right) \tag{2.10}$$

which is valid for $a \leq x \leq L$. The free end $0 \leq x \leq a$ has linear deflection, determined by the deflection and angle of the pipette at the point load and the length of the remaining free end

$$w(x) = w(a) - (a-x)w'(a) \tag{2.11}$$

So, the solutions for both sections of the pipette, which are separated by the point load, were

$$w(x) = \left\{ \begin{array}{ll} \frac{32F}{3\pi E}\left(\frac{L(a-L)^2(a(2D_1(L-x)-3D_2L+2D_2x)+L(2D_1(x-L)+D_2x))}{D_2^3(a(D_2-D_1)+D_1L)^2}\right) & \text{for } 0 \leq x < a \\ \frac{32F}{3\pi E}\left(\frac{L(L-x)^2(a(2D_1(L-x)+D_2(L+2x))+L(2D_1(x-L)-3D_2x))}{D_2^3(D_1(L-x)+D_2x)^2}\right) & \text{for } a \leq x \leq L \end{array} \right\}$$

To compensate for the inaccuracy of the assumed boundary conditions, we performed 15 calibrations on five random pipettes using a common method [57]. We hung a copper wire of known weight on each pipette and measured the distance from the applied weight to the tip (a) and the tip deflection (δ_{max}) (Figure 2.3). During calibration, deflections were measured as positive downward, so the relationship between $w(x)$ and $\delta(x)$ should be noted

$$\begin{aligned} |\delta_{max}| &= |w_{max}| = |w(0)| && (2.12) \\ &= \frac{32F}{3\pi E}\left(\frac{L^2(a-L)^2(-2aD_1+3aD_2+2D_1L)}{D_2^3(a(D_2-D_1)+D_1L)^2}\right) && (2.13) \end{aligned}$$

which was rearranged to get an expression for the elastic modulus (E)

$$E = \frac{1}{\delta_{max}}\frac{32F}{3\pi}\left(\frac{L^2(a-L)^2(-2aD_1+3aD_2+2D_1L)}{D_2^3(a(D_2-D_1)+D_1L)^2}\right) \tag{2.14}$$

Using Equation 2.14, an elastic modulus (mean ± SD) was calculated for the pipettes of 32.03 ± 1.33 GPa. This value was used to calculate force measurements during testing with Equation 2.15. After fabrication, the pipettes were coated in Cell-Tak using the adsorption method in the Corning Cell-Tak Cell and Tissue Adhesive *Instructions for Use*. Cell-Tak is a cellular adhesive derived from proteins of the marine mussel, *Mytilus edulis*, and has been shown to have no significant effect on cellular function [3, 20]. The pipettes were stored at 4°C and used within three weeks after coating.

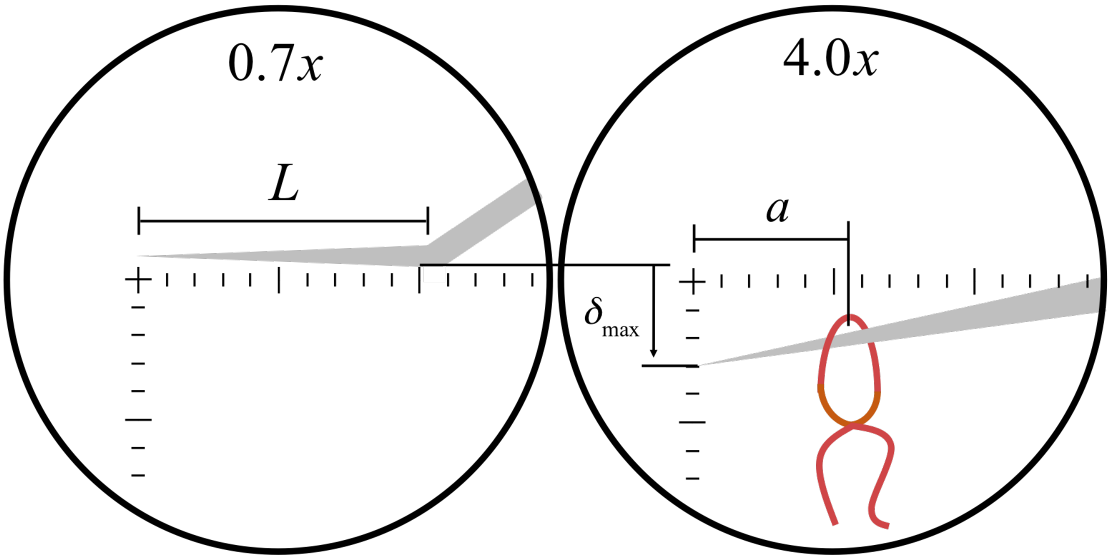

Figure 2.3: Graphical representation of pipette calibration using the microforge and a thin copper wire of known weight. The pipette cantilevers were so long they had to be measured on the lowest magnification (left), while maximum deflection and distance from the weight to the pipette tip were measured using the highest magnification on the microforge (right). Using this method, we calculated an elastic modulus for the pipette with Equation 2.14.

2.3 Contraction & Identification

Although the preparation of our SMCs of passage 1 and passages 4-6 matches protocols of other studies which compare contractile and synthetic SMCs [30, 37, 44], respectively, we avoid this naming convention for our cells because no protein analyses were performed, which is the most accurate identification method. Instead, to identify our SMCs, we measure their response to serotonin, which is another clear indicator of phenotype. Specifically, contractile SMCs show dramatic changes in size and shape when activated with a contraction agonist such as serotonin [40], while the response in synthetic SMCs is muted or absent. Synthetic SMCs are also larger in size than contractile SMCs [52], so we also compared undeformed cell diameters as another indicator of phenotype.

To perform the contraction experiments, we placed cells on the thermoplate above the inverted microscope and replaced the full media with 16.6 μM serotonin dissolved in DMEM.

Image data were taken at 0.32 frames per second and analyzed to measure changes in major axis length (ΔL) and cell area (ΔA) after 40 minutes of exposure. Results will be compared against contraction data for vascular SMCs in section 4.1.

In addition to comparing morphological differences between vaginal and vascular SMC contraction, these activation trials were used as training to help visually recognize SMCs. This method of SMC identification is common because it is time and cost effective, compared to the prohibitive expense of live cell sorting or other protein assays. The cultures were mainly composed of SMCs and fibroblasts, the latter of which do not dramatically respond to the agonist [2]. Because SMCs were the only cells in the culture activated by serotonin, the morphology of all responding cells were reviewed for common features, which were then used to visually identify SMCs for experiments.

2.4 Mechanical Testing

These experiments explore the effects of passaging and exposure to HBSS$^-$ on the tensile properties of vaginal SMCs. The exposure groups were defined as cells subject to 20, 40, 60, or >60 minutes of submersion time in HBSS$^-$ before performing the tensile test. Two groups were defined to compare passage effects. The first passage group included cells taken from the first passage and tested within five days of isolation. The second passage group included cells tested from passages 4-6. A single SMC may belong to both an exposure group and a passage group.

Immediately before testing, full media was replaced with HBSS$^-$ and the petri dishes with cells were placed on the 37°C thermoplate above the inverted microscope. Vaginal SMCs were identified by their fusiform, or spindle-like, shape and cells with their major axes perpendicular to the pipettes were selected for testing, such that we consistently loaded cells along their major axes. Once a target cell was chosen, flexible and stiff pipettes were gently lowered onto the cell membrane using the micromanipulators. Contact between the pipette tips and the cell was confirmed by slight indentation of the cellular membrane. After waiting 15 minutes for reliable adhesion, the cell was carefully lifted several microns from the substrate. Finally, the displacement of the stiff pipette was controlled by the piezoelectric actuator while the flexible pipette remained stationary.

For all experiments, the stiff pipette was subjected to a displacement rate of 0.25 μm s^{-1} and data collection was terminated when adhesion between one of the pipettes and the cell failed. The high-resolution camera was used with the inverted microscope to collect images of the cell during experiments at five frames per second.

2.5 Data Analysis

Analysis of image data was performed using ImageJ (National Institutes of Health, Bethesda, Maryland, USA) and the open-source software Tracker [64], a video analysis and modeling tool. The conversion factor between pixels and microns was determined by viewing a micro-grid array (R1L3S3P, ThorLabs) with the inverted microscope. For contraction experiments, ImageJ was used to measure changes in length (ΔL) and area (ΔA) during the test.

For mechanical experiments, ImageJ was used to measure the distance from the cell to the pipette tip (a), undeformed cell diameter (d_C), and undeformed cell length between pipettes (S_0). Tracker was used to measure deflection of the flexible pipette (δ_{max}) for each frame during the experiment. An edge of the flexible pipette was usually selected for tracking and the position data were imported and analyzed using MATLAB, which converted δ_{max} into force (F) with the following equation derived in subsection 2.2.1

$$F = \frac{3\pi E}{32}\delta_{max}\left(\frac{D_2^3(a(D_2 - D_1) + D_1L)^2}{L^2(a-L)^2(-2aD_1 + 3aD_2 + 2D_1L)}\right) \tag{2.15}$$

where E was our calculated value of the elastic modulus for the pipettes, 32.03 $\pm$ 1.33 GPa. Cell cross-sections perpendicular to the loading direction were assumed to be circular and force measurements were converted into stress (σ) using

$$\sigma = \frac{F}{A} = \frac{4F}{\pi d_C^2} = \frac{3E}{8d_C^2}\delta_{max}\left(\frac{D_2^3(a(D_2 - D_1) + D_1L)^2}{L^2(a-L)^2(-2aD_1 + 3aD_2 + 2D_1L)}\right) \tag{2.16}$$

Cell displacement (S) was calculated to be the controlled displacement of the stiff pipette minus the deflection of the flexible pipette

$$S = \Delta P - \delta_{max} \tag{2.17}$$

where ΔP is the controlled displacement of the piezoelectric actuator and stiff pipette and δ_{max} is the deflection of the flexible pipette, measured with Tracker (Figure 2.4). Engineering strain (ϵ) was calculated from cell displacement

$$\epsilon = \frac{S - S_0}{S_0} = \frac{\Delta P - \delta_{max} - S_0}{S_0} \tag{2.18}$$

Because cells are a biological system and likely have a non-linear stress-strain relationship, we report two different elastic moduli, E_{init} and E_{tot}. The initial moduli (E_{init}) were calculated using stress-strain data up to 10% strain, while the total moduli (E_{tot}) were calculated using stress-strain data up to the strain at which the cell detached from a pipette. Both moduli were calculated using least squares linear regression and fitting the equation of a line ($\sigma = E\epsilon$) to the stress-strain data, while forcing the fitted line through the origin.

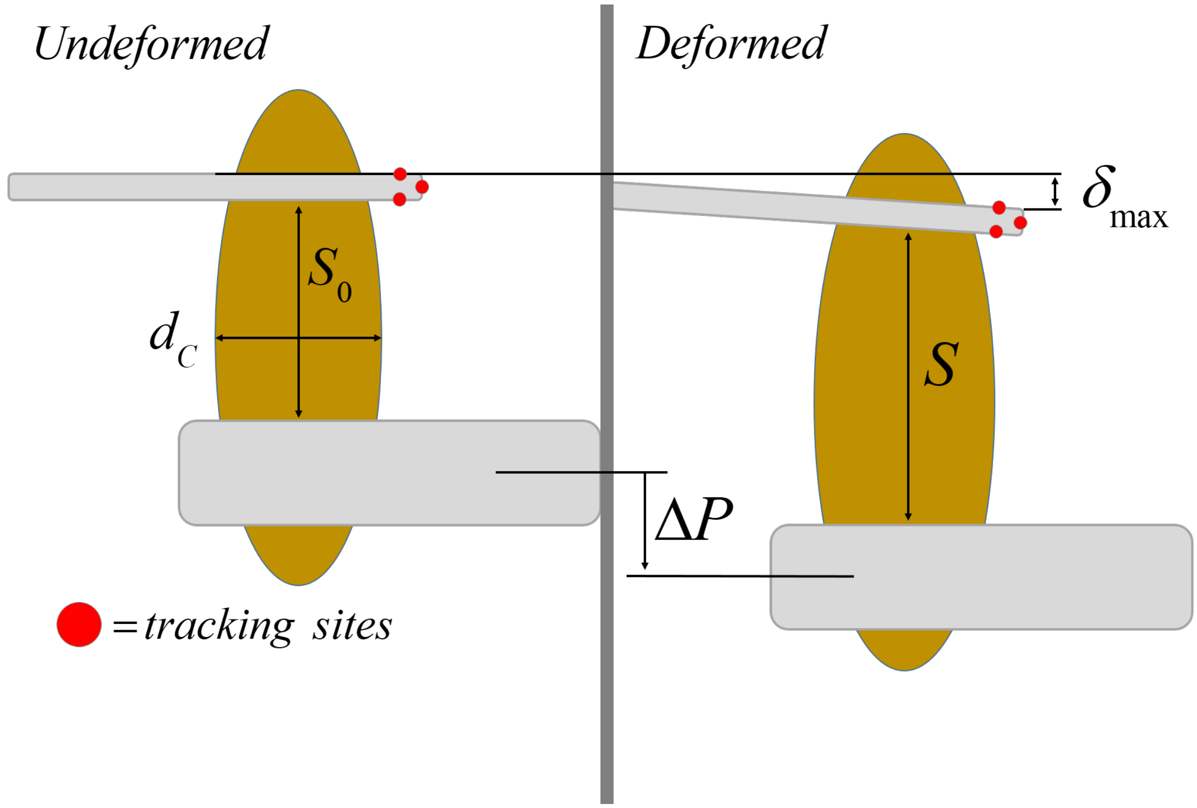

Figure 2.4: Graphical representation of collected image data, with labelled dimensions of interest. Cells were removed from the substrate and considered undeformed when no load was applied (left). As they are loaded, image data were used to measure maximum deflection of the flexible pipette using Tracker (right).

2.6 Statistics

The linear elastic moduli values E_{init} and E_{tot} were used to calculate the mean $\pm$ standard error of the mean (SEM) of stress-strain data. The moduli for each experiment were weighted equally for comparison, despite variations in maximum strain. Normality was confirmed with a published MATLAB package [46]. Using MATLAB, groups were compared using analysis of variance (ANOVA) and post hoc comparison. Differences were considered significant if $p < 0.1$. Power analyses were also performed using the MATLAB function *sampsizepwr*.

Chapter 3

Results

From the cells submerged in serotonin, 26 were analyzed and 15 were observed to significantly respond to the contraction agonist serotonin. After 40 minutes of serotonin exposure, changes in cell length (ΔL) and area (ΔA) between passage groups were significantly different (Table 3.2). Specifically, cells of higher passage numbers were significantly less responsive to the serotonin than cells of lower passage numbers (Figure 3.1).

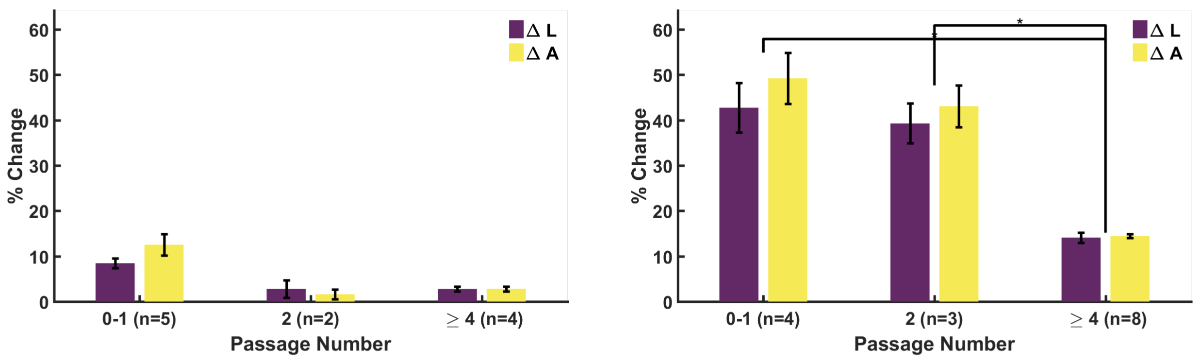

(a) (b)

Figure 3.1: Changes in vaginal SMC length (ΔL) and area (ΔA) after being activated with 16.6 μM serotonin. (a) Cells which were unresponsive to the contraction agonist and (b) cells that significantly responded. Of the cells that significantly responded, changes in both length (ΔL) and area (ΔA) were significantly greater for cells of passage groups 0-1 and 2, compared to cells with passage numbers greater than 4

Table 3.1: Summary of vaginal SMC response to 16.6 μM serotonin, a common contraction agonist, measured 40 minutes after exposure. Table includes cells which significantly contracted to the serotonin.

Passage Number	n	ΔL (%)	ΔA (%)
0-1	4	42.7 ± 5.5	49.2 ± 5.6
2	3	39.3 ± 4.4	43.1 ± 4.6
≥4	8	14.1 ± 1.1	14.5 ± 0.4
Differences		p (ΔL)	p (ΔA)
0-1 vs. ≥4		0.01413	0.00228
2 vs. ≥4		0.04864	0.01678

3.1 Tensile Test Results

Using the tensile testing protocol described in section 2.4, 16 SMCs were mechanically tested. Each cell was characterized by its passage number and its exposure time to $HBSS^-$ and assigned to a passage and an exposure group, such that one cell belonged to two groups. Stress-free cell diameters for vaginal SMCs from passage 1 (n=7) was 24.74 ± 1.04 μm and from passages 4-6 (n=9) was 22.63 ± 0.53 μm. For the exposure groups of 20 (n=4), 40 (n=5), 60 (n=3), and greater than 60 (n=4) minutes, stress-free cell diameters were 21.75 ± 2.03 μm, 22.68 ± 1.38 μm, 21.98 ± 1.06 μm, and 27.63 ± 0.65 μm, respectively. The differences in cell size between all pairs of groups were not statistically significant. For all cells, initial spacing between pipettes was 27.36 ± 0.71 μm, which was approximately 30% of the average major axis length of vaginal SMCs when adhered to a substrate. When adhesion failed, cells detached from the flexible pipettes in over 70% of cases. All cells exhibited initial and total elastic moduli of 6.06 ± 0.26 kPa and 5.4 ± 0.24 kPa, respectively. In every group, except cells subject to 40 minutes of $HBSS^-$ exposure, the total elastic modulus was lower than the initial modulus.

Stress-strain curves for all experiments are presented (Figure 3.2a). The maximum stress applied during loading was just greater than 4 kPa and maximum induced strain was near 100% of the original length, which occurred during the same experiment on a cell from passage 4 with 40 minutes of $HBSS^-$ exposure. For simpler data visualization, the mean ± SEM stress of all experiments is also presented at intervals of 1% strain up to 10% strain, which all cells achieved (Figure 3.2b). This type of representation was also used to compare of passage and exposure groups (Figure 3.3a & Figure 3.4a), respectively.

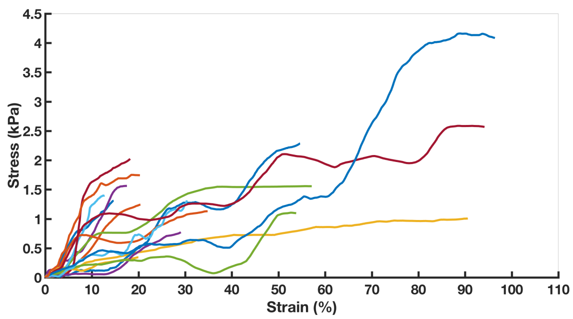

(a)

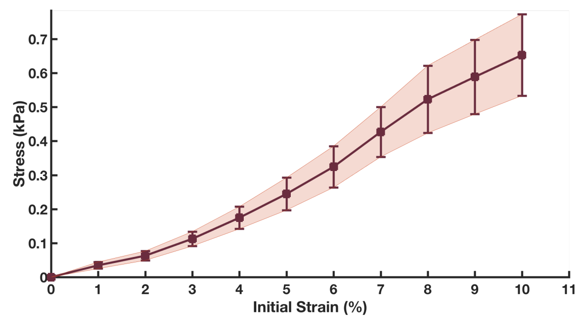

(b)

Figure 3.2: (a) Stress-strain data for all 16 cells subjected to tensile testing at a displacement rate of 0.25 μm s^{-1}. (b) Mean ± SEM stress for all 16 cells, taken at intervals of 1% strain, until 10% strain. This strain region represents the range used to calculated the initial elastic moduli (E_{init}).

3.1.1 Passage Results

To graphically represent the difference in elasticity between SMC passage groups, the averaged stress-strain curves and the mean elastic modulus of each group are presented (Figure 3.3a). Specifically, data from each group are expressed as a mean ± SEM stress, again taken at intervals of 1% strain until 10%. Variability increases as strain increases, with a relatively similar trend observed in each group. Cells from passage 1 (n=7) and passages 4-6 (n=9) had mean initial elastic moduli of 5.07 ± 0.71 kPa and 6.83 ± 0.39 kPa, respectively (Figure 3.3b). The total elastic moduli of cells from passage 1 and passages 4-6 were 3.48 ± 0.49 kPa and 6.89 ± 0.38 kPa, respectively. The difference in total elastic moduli between passage groups was significant (p=0.07221), with a statistical power (B) of 0.99126.

3.1.2 HBSS^{-} Exposure Results

Similar to the passage groups, differences in elasticity between cells subject to different HBSS^{-} exposure times are graphically presented with an averaged stress-strain curve (Figure 3.4a), as well as the mean elastic moduli for each group. The initial elastic moduli from cells subject to 20 (n=4), 40 (n=5), 60 (n=3), and greater than 60 (n=4) minutes of HBSS exposure were 8.26 ± 1.3 kPa, 5.27 ± 0.84 kPa, 4.81 ± 1.28 kPa, and 5.78 ± 1.02 kPa, respectively (Figure 3.4b). The total elastic moduli from cells subject to 20, 40, 60, and greater than 60 minutes of exposure were 7.77 ± 1.02 kPa, 5.64 ± 0.82 kPa, 4.33 ± 1.74 kPa, and 3.53 ± 0.08 kPa, respectively. Although longer HBSS^{-} exposure time generally led to more compliant cells, differences between groups were not statistically significant. Cells subject 20 minutes of exposure exhibited the steepest stress-strain curve and failure occurred before 25% strain for each cell (Figure 3.4a).

Table 3.2: Summary of results of tensile tests on single vaginal SMCs, including initial cell diameters (d_C), initial elastic moduli (E_{init}), and total moduli (E_{tot}). Data values are presented as mean ± SEM.

Passage Number	n	d_C (μm)	E_{init} (kPa)	E_{tot} (kPa)
1	7	24.74 ± 1.04	5.07 ± 0.71	3.48 ± 0.49
4-6	9	22.63 ± 0.53	6.83 ± 0.39	6.89 ± 0.38
HBSS^{-} Exposure Time (min)				
20	4	21.75 ± 2.03	8.26 ± 1.3	7.77 ± 1.02
40	5	22.68 ± 1.38	5.27 ± 0.84	5.64 ± 0.82
60	3	21.98 ± 1.06	4.81 ± 1.28	4.33 ± 1.74
>60	4	27.63 ± 0.65	5.78 ± 1.02	3.53 ± 0.08

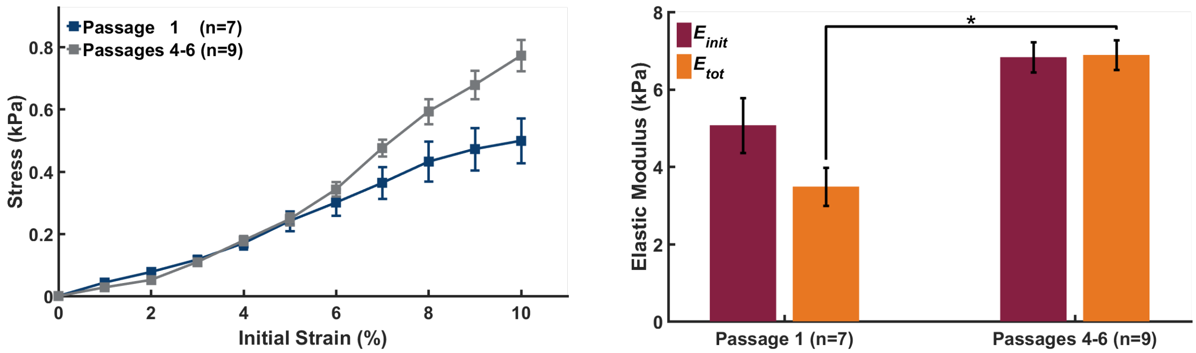

(a) (b)

Figure 3.3: (a) Mean ± SEM stress for vaginal SMCs from passage 1 versus passages 4-6, taken at intervals of 1% strain, until 10% strain. (b) Initial (E_{init}) and total (E_{tot}) elastic moduli versus passage number. The total elastic modulus of passage 1 cells was significantly (p=0.07221) lower than the modulus for cells from passages 4-6.

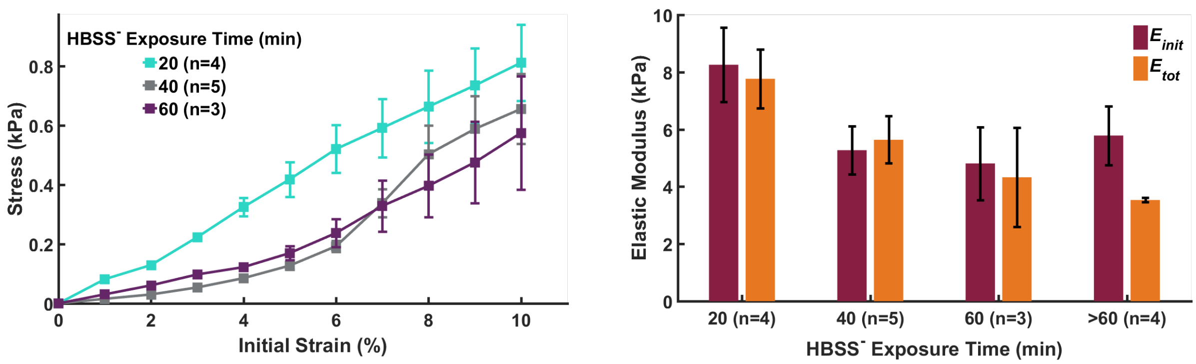

(a) (b)

Figure 3.4: (a) Mean ± SEM stress for vaginal SMCs from different HBSS^{-} exposure times, taken at intervals of 1% strain, until 10% strain. (b) Initial (E_{init}) and total (E_{tot}) elastic moduli versus exposure time. There were no statistically significant differences between any pair of exposure groups.

Chapter 4

Discussion

Results of the current experiment represent novel data on the elastic moduli of single vaginal SMCs. Because no current studies report the material properties of vaginal SMCs, we compare our results against other types of SMCs. Differences in elastic moduli are to be expected among SMCs of different types and from different species, but comparing with results from other studies still provides a useful measure of validity.

The values of our initial and total elastic moduli, 6.06 ± 0.26 kPa and 5.4 ± 0.24 kPa, respectively, fall within the range of published data on various types of SMCs [29, 56]. The elastic moduli for human airway, rat aortic, and human uterine SMCs are roughly 15 kPa [32], 5 kPa [56], and 11 kPa [13], respectively, which are similar in magnitude to our calculated value, but vary based on phenotype, prestress, and activation.

4.1 Effect of Passage Number

As mentioned in section 2.3, SMCs from passage 1 and passages 4-6 likely correspond to contractile and synthetic SMCs, respectively, according to other studies [30, 37, 41, 44]. We confirmed a difference in phenotypic expression between our two passage groups by comparing their sizes and contraction, the latter of which was significantly different for passage groups.

The difference in elastic moduli between passage groups is opposite to what has been observed in vascular SMCs. Specifically, contractile vascular SMCs have been measured to be significantly stiffer than synthetic ones [30, 44], by up to factor of three. The differences in elasticity were attributed to changes in the actin and myosin filament network, commonly referred to as the contractile apparatus, which is much less robust in synthetic SMCs [37, 41]. These filaments, collectively called stress fibers, are at least partially responsible for cell contraction, according to the sliding filament theory [19, 61]. The hypothesis was that the stress fibers of synthetic SMCs, which are thinner and fewer in number, are less able to resist deformation, leading to more compliant cells. This hypothesis seems valid, but we extend the discussion to consider another difference between contractile and synthetic SMCs.

Synthetic SMCs also exhibit a greater density of organelles per cell, especially the Golgi and rough endoplasmic reticulum (RER) [2]. The architecture of the contractile apparatus and its relation to organelles are critical factors for understanding the mechanical response of SMCs and it is known that the apparatus adheres directly to the nucleus, instead of circumventing it [26]. Of two different cells, stress fibers in the more densely packed organelle cell will have a shorter average length, due to the presence of the organelles. Assuming, like the nucleus, that other organelles are stiffer than stress fibers, identical stretching will lead to greater strain in each individual fiber of the more populated cell, leading to greater force production

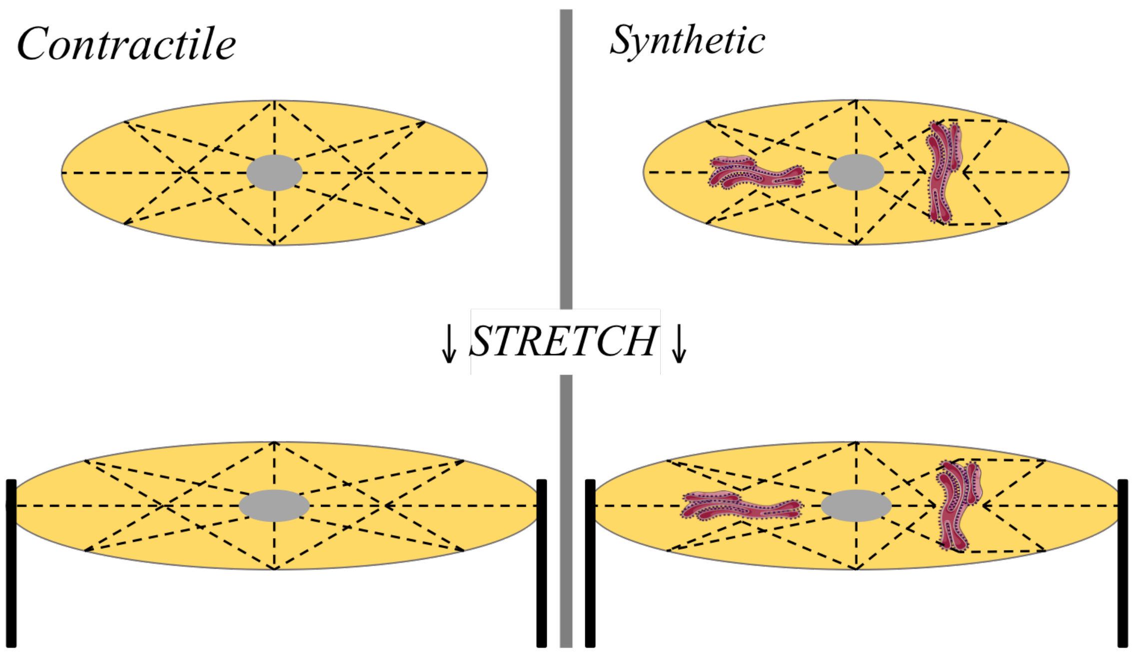

Figure 4.1: Graphical representation of a contractile SMC compared to a synthetic SMC, which has more organelles. Identical stretching will lead to greater strain in each individual fiber of the synthetic cell.

compared to the cell with fewer organelles (Figure 4.1). Because the composition of synthetic cells includes a higher density of stiffer components, they should exhibit a higher stiffness than contractile cells.

This hypothesis describes the mechanism through which synthetic SMCs would have a higher elastic moduli than contractile SMCs, as observed in the current study. As mentioned previously, however, there remains the opposing effect of less resilient stress fibers in synthetic SMCs. Among other factors, differences in elasticity between SMC phenotypes will depend on the magnitude of each effect. Although SMCs of different types and species share some characteristics, it remains to be proven if all phenotype differences for other SMCs are also true for vaginal SMCs, such as the change in stress fiber quality. Generally, how phenotype differences between contractile and synthetic SMCs translate into contrasting mechanical properties is not well understood.

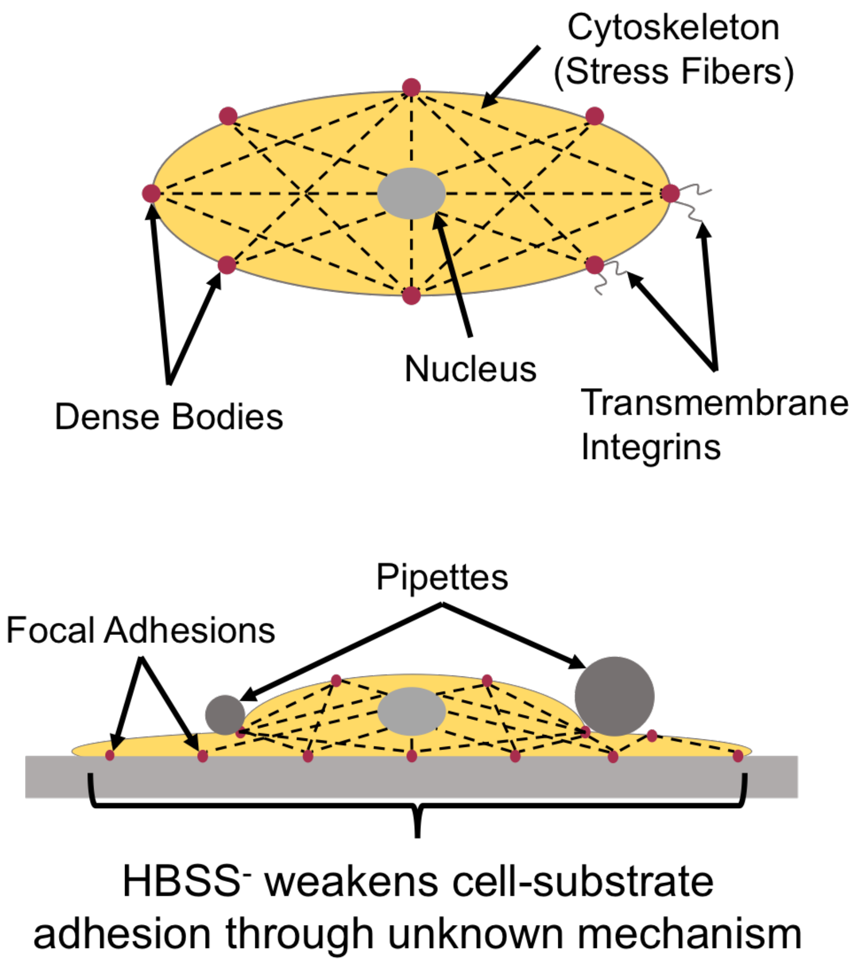

Figure 4.2: Basic representation of the structure of an SMC (top), including a side-view of a cell adhered to a substrate, with pipettes in position to lift the cell from the substrate (bottom).

4.2 Effect of HBSS$^-$ Exposure

In general, longer HBSS$^-$ exposure time led to more compliant cells. The commonly used testing media weakens the adhesion between SMCs and their substrate, but the mechanism of this effect is unknown and may affect their mechanical response.

Tension in SMCs is supported in part by the cytoskeleton throughout the cell and force is transmitted to the extracellular environment *via* transmembrane integrins, which are extruded from dense plaque bodies on the cell membrane [15, 21, 54]. When an SMC is adhered to a substrate, these dense bodies form focal adhesions, to which the stress fibers consolidate (Figure 4.2). Another component of SMC force production, however, is the active remodeling of the cytoskeletal lattice [14, 27], referred to as glassy dynamics. Through similar mechanisms used by SMCs to migrate, tension is supported by first molding their membrane to the environment, stiffening their membrane, and then increasing and maintaining force *via* the sliding filament theory [11]. During this process, stress fibers are consolidated among the dense plaque bodies to create fewer, but larger focal adhesions, through which force is transmitted to the environment [40]. If HBSS^{-} affects the adhesion between a cell and a pipette in a similar way it affects the adhesion between a cell and a substrate, it may compromise the cell's ability to support force using its cytoskeleton, increasing compliance.

Previous observations suggest that glassy dynamics are critical for force production in SMCs, perhaps for the purpose of prestressing the contractile apparatus or stress fibers. Cells with prestress will expend less energy generating the same force compared to a cell without prestress. These two components of force production and maintenance in SMCs, glassy dynamics and sliding filament activation, may exist to optimize energy performance. Cells that have been submerged in HBSS^{-} for a longer period of time may suffer damage to the cytoskeleton, transmembrane integrins, or dense plaque bodies as an unintended result of weakening their adhesion strength to the substrate, compromising their ability to support force using dynamic remodeling. We suspect this is why SMCs that have been submerged in HBSS^{-} for a longer period of time are more compliant.

4.3 Limitations

While some variability in the elastic moduli of our SMCs can be attributed to cell-to-cell variation, another source was the quality of the cell-pipette adhesion, which led to slippage, as seen in the stress-strain curves (Figure 3.2a). Cases of extreme slippage were qualitatively identified from image data and results from these tests were discarded, but minor slippage likely produced some noise in stress-strain curves. Additionally, failure most likely occurred at the flexible pipettes due to their higher curvature compared to the stiff pipettes, which allowed less contact area for adherence. The quality of adhesion between the cell and the pipettes was the greatest limitation of this protocol and current study.

Another source of experimental error was flow of the media within the petri dish from air ventilation in the lab. Small disturbances to the media surface were observed to influence the deflection of the flexible pipette. The effect was mitigated, but maybe not entirely eliminated, with a shielding fabric around the experimental setup.

4.4 Conclusions

Results from the current study suggest that passage number should be controlled in future experiments. Higher passage vaginal SMCs exhibited significantly higher total elastic moduli than lower passage SMCs, while exposure time to $HBSS^-$ had no statistically significant effect. Although the elasticity difference in phenotype is opposite to the trend for vascular SMCs, the results are not necessarily contradictory. The contraction of vaginal versus vascular SMCs is also dramatically different. When activated with serotonin, vascular SMCs increase in length along their major axes, while maintaining a constant cell area [40]. In contrast, vaginal SMCs reduced in both length and area by up to 70% when activated with the same agonist, as described in chapter 3. This disparity suggests fundamental differences in the production and maintenance of force between vaginal and vascular SMCs.

Another topic for which more data would be useful is the glassy dynamics of SMCs, for which there is a dearth of research. The cytoskeletal bonding sites on the cell membrane help regulate cell shape and migration and have been shown to respond to environmental cues such as mechanical and electrical stimuli and agonists like norepinephrine, histamine, and serotonin [12, 17, 24, 40, 66]. It remains unclear why SMCs dynamically change shape before activating their contractile apparatus, which may be critical information for future experiments.

In the present study, we established a protocol for performing mechanical tests on single vaginal SMCs and investigated the effect of two experimental factors: passage number and exposure time to $HBSS^{-}$. The modular nature of our testing setup allows relatively simple modifications to the protocol in order to investigate mechanical properties of single cells from other pelvic tissues and organs. Factors of interest include age, parity, BMI, and stage of POP. Our setup could be integrated with birefringence imaging techniques to view cell shape in three dimensions [9]. Pairing our tests with such an imaging system would allow us to measure changes in cell cross-section and obtain more accurate stress-strain data for future experiments.

Bibliography

[1] S. D. Abramowitch, A. Feola, Z. Jallah, and P. A. Moalli. Tissue mechanics, animal models, and pelvic organ prolapse: a review. *European Journal of Obstetrics and Gynecology and Reproductive Biology*, 144:S146–S158, 2009.

[2] J. A. Beamish, P. He, K. Kottke-Marchant, and R. E. Marchant. Molecular regulation of contractile smooth muscle cell phenotype: implications for vascular tissue engineering. *Tissue Engineering Part B: Reviews*, 16(5):467–491, 2010.

[3] C. V. Benedict and P. T. Picciano. Adhesives from marine mussels. In *Adhesives from Renewable Resources*, pages 465–483. ACS Publications, 1989.

[4] M. K. Boreham, R. T. Miller, J. I. Schaffer, and R. A. Word. Smooth muscle myosin heavy chain and caldesmon expression in the anterior vaginal wall of women with and without pelvic organ prolapse. *American Journal of Obstetrics & Gynecology*, 185(4): 944–952, 2001.

[5] M. K. Boreham, C. Y. Wai, R. T. Miller, J. I. Schaffer, and R. A. Word. Morphometric analysis of smooth muscle in the anterior vaginal wall of women with pelvic organ prolapse. *American Journal of Obstetrics & Gynecology*, 187(1):56–63, 2002.

[6] M. A. T. Bortolini, O. Shynlova, H. P. Drutz, R. A. Castro, M. J. B. C. Girao, S. Lye, and M. Alarab. Expression of genes encoding smooth muscle contractile proteins in

vaginal tissue of women with and without pelvic organ prolapse. *Neurourology and Urodynamics*, 31(1):109–114, 2012.

[7] J. T. Butcher, B. C. Barrett, and R. M. Nerem. Equibiaxial strain stimulates fibroblastic phenotype shift in smooth muscle cells in an engineered tissue model of the aortic wall. *Biomaterials*, 27(30):5252–5258, 2006.

[8] J. H. Chamley-Campbell and G. R. Campbell. What controls smooth muscle phenotype? *Atherosclerosis*, 40(3-4):347–357, 1981.

[9] S. Chen and Y. Zhu. Quantitative phase imaging of living cells with a swept laser source. In *Proc. of SPIE Vol*, volume 9718, pages 971827–1, 2016.

[10] A. T. Churchman and R. C. M. Siow. Isolation, culture and characterisation of vascular smooth muscle cells. *Angiogenesis Protocols: Second Edition*, pages 127–138, 2009.

[11] B. Fabry and J. J. Fredberg. Remodeling of the airway smooth muscle cell: are we built of glass? *Respiratory Physiology &; Neurobiology*, 137(2-3):109–124, 2003.

[12] F. S. Fay and C. M. Delise. Contraction of isolated smooth-muscle cells—structural changes. *Proceedings of the National Academy of Sciences*, 70(3):641–645, 1973.

[13] J. J. Glerum, R. Van Mastrigt, and A. J. Van Koeveringe. Mechanical properties of mammalian single smooth muscle cells iii. passive properties of pig detrusor and human a terme uterus cells. *Journal of Muscle Research & Cell Motility*, 11(5):453–462, 1990.

[14] S. J. Gunst and J. J. Fredberg. The first three minutes: smooth muscle contraction, cytoskeletal events, and soft glasses. *Journal of Applied Physiology*, 95(1):413–425, 2003.

[15] S. J. Gunst and D. D. Tang. The contractile apparatus and mechanical properties of airway smooth muscle. *European Respiratory Journal*, 15(3):600–616, 2000.

[16] A. J. Halayko and J. Solway. Invited review: molecular mechanisms of phenotypic plasticity in smooth muscle cells. *Journal of Applied Physiology*, 90(1):358–368, 2001.

[17] K. Hayashi. Tensile properties and local stiffness of cells. *Mechanics of Biological Tissue*, pages 137–152, 2006.

[18] M. Heidari, C. A. Mandato, and S. Lehoux. Vascular smooth muscle cell phenotypic modulation and the extracellular matrix. *Artery Research*, 9:14–18, 2015.

[19] H. E. Huxley. Fifty years of muscle and the sliding filament hypothesis. *The FEBS Journal*, 271(8):1403–1415, 2004.

[20] D. S. Hwang, S. B. Sim, and H. J. Cha. Cell adhesion biomaterial based on mussel adhesive protein fused with rgd peptide. *Biomaterials*, 28(28):4039–4046, 2007.

[21] D. E. Ingber. Tensegrity i. cell structure and hierarchical systems biology. *Journal of Cell Science*, 116(7):1157–1173, 2003.

[22] G. Iribe, M. Helmes, and P. Kohl. Force-length relations in isolated intact cardiomyocytes subjected to dynamic changes in mechanical load. *American Journal of Physiology-Heart and Circulatory Physiology*, 292(3):H1487–H1497, 2007.

[23] G. Iribe, C. W. Ward, P. Camelliti, C. Bollensdorff, F. Mason, R. A. B. Burton, A. Garny, M. K. Morphew, A. Hoenger, W. J. Lederer, and P. Kohl. Axial stretch of rat single ventricular cardiomyocytes causes an acute and transient increase in ca2+ spark rate. *Circulation Research*, 104(6):787–795, 2009.

[24] G. Iribe, T. Kaneko, Y. Yamaguchi, and K. Naruse. Load dependency in force–length relations in isolated single cardiomyocytes. *Progress in Biophysics and Molecular Biology*, 115(2):103–114, 2014.

[25] A. Kamgoué, J. Ohayon, and P. Tracqui. Estimation of cell young's modulus of adherent cells probed by optical and magnetic tweezers: influence of cell thickness and bead immersion. *Journal of Biomechanical Engineering*, 129(4):523–530, 2007.

[26] K. Kuo and C. Y. Seow. Contractile filament architecture and force transmission in swine airway smooth muscle. *Journal of Cell Science*, 117(8):1503–1511, 2004.

[27] R. E. Laudadio, E. J. Millet, B. Fabry, S. S. An, J. P. Butler, and J. J. Fredberg. Rat airway smooth muscle cell during actin modulation: rheology and glassy dynamics. *American Journal of Physiology-Cell Physiology*, 289(6):C1388–C1395, 2005.

[28] J. Y. Le Guennec, N. Peineau, J. A. Argibay, K. G. Mongo, and D. Garnier. A new method of attachment of isolated mammalian ventricular myocytes for tension recording: length dependence of passive and active tension. *Journal of Molecular and Cellular Cardiology*, 22(10):1083–1093, 1990.

[29] T. Matsumoto and K. Nagayama. Tensile properties of vascular smooth muscle cells: bridging vascular and cellular biomechanics. *Journal of Biomechanics*, 45(5):745–755, 2012.

[30] T. Matsumoto, J. Sato, M. Yamamoto, and M. Sato. Smooth muscle cells freshly isolated from rat thoracic aortas are much stiffer than cultured bovine cells: possible effect of phenotype. *JSME International Journal Series C: Mechanical Systems, Machine Elements and Manufacturing*, 43(4):867–874, 2000.

[31] T. Matsumoto, K. Nagayama, H. Miyazaki, and Y. Ujihara. Effects of cytoskeletal structures on elastic and viscoelastic properties of cells in soft tissues. *Biomechanics at Micro- and Nanoscale Levels*, 4:14–24, 2007.

[32] T. Matsumoto, S. Sugita, and K. Nagayama. Tensile properties of smooth muscle cells, elastin, and collagen fibers. In *Vascular Engineering*, pages 127–140. Springer, 2016.

[33] S. Mei, M. Ye, L. Gil, J. Zhang, Y. Zhang, K. Candiotti, and P. Takacs. The role of smooth muscle cells in the pathophysiology of pelvic organ prolapse. *Female Pelvic Medicine & Reconstructive Surgery*, 19(5):254–259, 2013.

[34] R. P. Metz, J. L. Patterson, and E. Wilson. Vascular smooth muscle cells: isolation, culture, and characterization. *Cardiovascular Development: Methods and Protocols*, pages 169–176, 2012.

[35] S. Meyer, C. Achtari, P. Hohlfeld, and L. Juillerat-Jeanneret. The contractile properties of vaginal myofibroblasts: Is the myofibroblasts contraction force test a valuable indication of future prolapse development? *International Urogynecology Journal*, 19(10): 1399–1403, 2008.

[36] H. Miyazaki, Y. Hasegawa, and K. Hayashi. A newly designed tensile tester for cells and its application to fibroblasts. *Journal of Biomechanics*, 33(1):97–104, 2000.

[37] Hiroshi Miyazaki, Yoshitaka Hasegawa, and Kozaburo Hayashi. Tensile properties of contractile and synthetic vascular smooth muscle cells. *JSME International Journal Series C Mechanical Systems, Machine Elements and Manufacturing*, 45(4):870–879, 2002.

[38] P. A. Moalli, N. S. Howden, J. L. Lowder, J. Navarro, K. M. Debes, S. D. Abramowitch, and S. L. Y. Woo. A rat model to study the structural properties of the vagina and its supportive tissues. *American Journal of Obstetrics & Gynecology*, 192(1):80–88, 2005.

[39] K. Nagayama and T. Matsumoto. Estimation of single stress fiber stiffness in cultured

aortic smooth muscle cells under relaxed and contracted states: its relation to dynamic rearrangement of stress fibers. *Journal of Biomechanics*, 43(8):1443–1449, 2010.

[40] K. Nagayama and T. Matsumoto. Dynamic change in morphology and traction forces at focal adhesions in cultured vascular smooth muscle cells during contraction. *Cellular and Molecular Bioengineering*, 4(3):348–357, 2011.

[41] K. Nagayama, Y. Nagano, M. Sato, and T. Matsumoto. Effect of actin filament distribution on tensile properties of smooth muscle cells obtained from rat thoracic aortas. *Journal of Biomechanics*, 39(2):293–301, 2006.

[42] K. Nagayama, S. Yanagihara, and T. Matsumoto. A novel micro tensile tester with feed-back control for viscoelastic analysis of single isolated smooth muscle cells. *Medical Engineering & Physics*, 29(5):620–628, 2007.

[43] K. Nagayama, A. Adachi, and T. Matsumoto. Heterogeneous response of traction force at focal adhesions of vascular smooth muscle cells subjected to macroscopic stretch on a micropillar substrate. *Journal of Biomechanics*, 44(15):2699–2705, 2011.

[44] K. Nagayama, S. Saito, and T. Matsumoto. Multiphasic stress relaxation response of freshly isolated and cultured vascular smooth muscle cells measured by quasi-in situ tensile test. *Bio-Medical Materials and Engineering*, 25(3):299–312, 2015.

[45] P. Norton, C. Boyd, and S. Deak. Collagen synthesis in women with genital prolapse or stress urinary incontinence. *Neurourology and Urodynamics*, 11:300–1, 1992.

[46] M. Öner and I. D. Kocakoç. Jmasm 49: A compilation of some popular goodness of fit tests for normal distribution: Their algorithms and matlab codes (matlab). *Journal of Modern Applied Statistical Methods*, 16(2):30, 2017.

[47] G. K. Owens, M. S. Kumar, and B. R. Wamhoff. Molecular regulation of vascular smooth muscle cell differentiation in development and disease. *Physiological Reviews*, 84(3):767–801, 2004.

[48] S. Poncet, S. Meyer, C. Richard, J. Aubert, and L. Juillerat-Jeanneret. The expression and function of the endothelin system in contractile properties of vaginal myofibroblasts of women with uterovaginal prolapse. *American Journal of Obstetrics & Gynecology*, 192(2):426–432, 2005.

[49] S. L. Rose and J. E. Babensee. Complimentary endothelial cell/smooth muscle cell co-culture systems with alternate smooth muscle cell phenotypes. *Annals of Biomedical Engineering*, 35(8):1382–1390, 2007.

[50] A. M. Ruiz-Zapata, M. H. Kerkhof, B. Zandieh-Doulabi, H. A. M. Brölmann, T. H. Smit, and M. N. Helder. Functional characteristics of vaginal fibroblastic cells from premenopausal women with pelvic organ prolapse. *Molecular Human Reproduction*, 20 (11):1135–1143, 2014.

[51] A. M. Ruiz-Zapata, M. H. Kerkhof, S. Ghazanfari, B. Zandieh-Doulabi, R. Stoop, T. H. Smit, and M. N. Helder. Vaginal fibroblastic cells from women with pelvic organ prolapse produce matrices with increased stiffness and collagen content. *Scientific Reports*, 6: 22971, 2016.

[52] E. M. Rzucidlo, K. A. Martin, and R. J. Powell. Regulation of vascular smooth muscle cell differentiation. *Journal of Vascular Surgery*, 45(6):A25–A32, 2007.

[53] G. Shue and F. V. Brozovich. The frequency response of smooth muscle stiffness during ca 2+-activated contraction. *Biophysical Journal*, 76(5):2361–2369, 1999.

[54] J. V. Small and M. Gimona. The cytoskeleton of the vertebrate smooth muscle cell. *Acta Physiologica Scandinavica*, 164(4):341–348, 1998.

[55] P. G. Smith, C. Roy, S. Fisher, Q. Huang, and F. Brozovich. Selected contribution: mechanical strain increases force production and calcium sensitivity in cultured airway smooth muscle cells. *Journal of Applied Physiology*, 89(5):2092–2098, 2000.

[56] D. Stamenović. Cytoskeletal mechanics in airway smooth muscle cells. *Respiratory Physiology & Neurobiology*, 163(1-3):25–32, 2008.

[57] S. Sugiura, S. Nishimura, S. Yasuda, Y. Hosoya, and K. Katoh. Carbon fiber technique for the investigation of single-cell mechanics in intact cardiac myocytes. *Nature Protocols*, 1(3):1453–1457, 2006.

[58] V. W. Sung, R. G. Rogers, J. I. Schaffer, E. M. Balk, K. Uhlig, J. Lau, H. Abed, T. L. Wheeler, M. Y. Morrill, J. L. Clemons, D. D. Rahn, J. C. Lukban, L. Lowenstein, K. Kenton, and S. B. Young. Graft use in transvaginal pelvic organ prolapse repair: a systematic review. *Obstetrics & Gynecology*, 112(5):1131–1142, 2008.

[59] P. Takacs, M. Gualtieri, M. Nassiri, K. Candiotti, and C. A. Medina. Vaginal smooth muscle cell apoptosis is increased in women with pelvic organ prolapse. *International Urogynecology Journal*, 19(11):1559, 2008.

[60] P. Takacs, Y. Zhang, S. Jaramillo, T. Bardawil, K. Candiotti, and C. A. Medina. The effects of estrogen, progesterone and polypropylene mesh on vaginal smooth muscle cell proliferation. *Journal of Smooth Muscle Research*, 46(1):9–15, 2010.

[61] T. Tan and R. De Vita. A structural constitutive model for smooth muscle contraction in biological tissues. *International Journal of Non-Linear Mechanics*, 75:46–53, 2015.

[62] O. Thoumine and A. Ott. Time scale dependent viscoelastic and contractile regimes in fibroblasts probed by microplate manipulation. *Journal of Cell Science*, 110(17): 2109–2116, 1997.

[63] J. Thyberg, U. Hedin, M. Sjölund, L. Palmberg, and B. A. Bottger. Regulation of differentiated properties and proliferation of arterial smooth muscle cells. *Arteriosclerosis, Thrombosis, and Vascular Biology*, 10(6):966–990, 1990.

[64] Aaron Titus. Tracker lab manual and workshop resources, June 2012.

[65] J. Tock, V. Van Putten, K. R. Stenmark, and R. A. Nemenoff. Induction of sm-α-actin expression by mechanical strain in adult vascular smooth muscle cells is mediated through activation of jnk and p38 map kinase. *Biochemical and Biophysical Research Communications*, 301(4):1116–1121, 2003.

[66] N. Wang, I. M. Tolic-Nørrelykke, J. Chen, S. M. Mijailovich, J. P. Butler, J. J. Fredberg, and D. Stamenovic. Cell prestress. i. stiffness and prestress are closely associated in adherent contractile cells. *American Journal of Physiology-Cell Physiology*, 282(3): C606–C616, 2002.

[67] S. Wang, Z. Zhang, D. Lü, and Q. Xu. Effects of mechanical stretching on the morphology and cytoskeleton of vaginal fibroblasts from women with pelvic organ prolapse. *International Journal of Molecular Sciences*, 16(5):9406–9419, Apr 2015. ISSN 1422-0067. doi: 10.3390/ijms16059406. URL http://dx.doi.org/10.3390/ijms16059406.

[68] T. Wannenburg, G. H. Heijne, J. H. Geerdink, H. W. Van den Dool, P. M. L. Janssen, and P. P. De Tombe. Cross-bridge kinetics in rat myocardium: effect of sarcomere length and calcium activation. *American Journal of Physiology-Heart and Circulatory Physiology*, 279(2):H779–H790, 2000.

[69] B. Williams. Mechanical influences on vascular smooth muscle cell function. *Journal of Hypertension*, 16(12):1921–1929, 1998.

[70] S. Yasuda, S. Sugiura, N. Kobayakawa, H. Fujita, H. Yamashita, K. Katoh, Y. Saeki, H. Kaneko, Y. Suda, R. Nagai, and H. Sugi. A novel method to study contraction characteristics of a single cardiac myocyte using carbon fibers. *American Journal of Physiology-Heart and Circulatory Physiology*, 281(3):H1442–H1446, 2001.

[71] W. Zong, Z. C. Jallah, S. E. Stein, S. D. Abramowitch, and P. A. Moalli. Repetitive mechanical stretch increases extracellular collagenase activity in vaginal fibroblasts. *Female Pelvic Medicine & Reconstructive Surgery*, 16(5):257, 2010.